Asymmetrically Charged Carbon Nanotubes by Controlled Functionalization

Qiang Peng,[†] Liangti Qu,[†] Liming Dai,[†,*] Kyoungweon Park,[‡] and Richard A. Vaia[‡,*]

[†]Departments of Materials Engineering and Chemistry and UDRI, University of Dayton, 300 College Park, Dayton, Ohio 45469, and [‡]Materials and Manufacturing Directorate, Air Force Research Laboratory, AFRL/RXBN, Wright-Patterson AFB, Ohio 45433

ABSTRACT Surface modification of carbon nanotubes (CNTs) has been widely studied for some years. However, the asymmetric modification of individual CNTs with different molecular species/nanoparticles at the two end-tips or along the nanotube length is only a recent development. As far as we are aware, no attempt has so far been made to *asymmetrically* functionalize individual CNTs with moieties of opposite charges. In this paper, we have demonstrated a simple, but effective, asymmetric modification of the sidewall of CNTs with oppositely charged moieties by plasma treatment and $\pi-\pi$ stacking interaction. The *as-prepared* asymmetrically sidewall-functionalized CNTs can be used as a platform for bottom-up self-assembly of complex structures or can be charge-selectively self-assembled onto and/or between electrodes with specific biases under an appropriate applied voltage for potential device applications.

KEYWORDS: carbon nanotube · asymmetric functionalization · selective charge · self-assembly

Since Iijima's report in 1991,[1] carbon nanotubes (CNTs) have attracted a great deal of interest for a wide range of potential applications, including use in optoelectronic devices, biomedical systems, and polymer nanocomposites.[1−10] It has been recognized that surface characteristics of CNTs are of paramount importance for these and many other applications. This is because the use of CNTs in optoelectronic devices often requires that they be self-assembled into various functional structures onto a substrate through the nanotube surface−surface and/or nanotube surface−substrate interactions. Likewise, it is the nanotube surface that comes into direct contact with the physiological environment in biomedical systems and polymer matrix in nanocomposites. These interfacial contacts play an important role in regulating performance of the nanotube-based multicomponent materials and devices. However, it is difficult, if not impossible, to synthesize CNTs with desirable surface properties that are demanded for all of their potential applications. Therefore, surface modification and interfacial engineering are essential in making functionalized CNTs of tailor-made surface characteristics required for specific applications. Consequently, a number of intriguing covalent and noncovalent approaches have been devised for functionalization of CNTs.[11−17] While a large variety of (macro)molecular species can be covalently linked to the nanotube surface *via* various chemical reactions,[16] the covalent chemistry suffers the major drawback of detrimentally destructing the nanotube graphitic structure.[17] On the other hand, the number of functional moieties that can be introduced onto the surface of CNTs using the "nondestructive" noncovalent adsorption is largely limited by certain aromatic molecules and their derivatives with a planar π-moiety (*e.g.*, pyrene) of strong interaction with the basal plane of graphite on the nanotube sidewall *via* $\pi-\pi$ stacking.[18−21] In addition, certain synthetic polymers, proteins, and DNA chains have also been demonstrated to noncovalently wrap the nanotube sidewall.[22−24] Additionally, the wrapping of CNTs with charged macromolecules (*e.g.*, polyelectrolytes) for electrostatic assembling has been explored.[25−33]In a vast majority of CNT interfacial modification studies, spatially homogeneous functionalization results; that is, a tube is uniformly encased by an organic corona. Although many objects, such as reinforcement of polymers or ceramics, require uniformity, many others, including sensors, actuators, and M&NEMS, would benefit from site-specific surface modification with structural periodicity on a scale of an individual CNT. Controllably confining functions to different regions of a CNT further expands its utility as a nanoscale building block for bottom-up assembly.

Some interesting chemistries of CNTs have recently been reported to address the

*Address correspondence to ldai@udayton.edu, Richard.Vaia@wpafb.af.mil.

Received for review April 29, 2008 and accepted August 11, 2008.

Published online August 28, 2008.
10.1021/nn8002532 CCC: $40.75

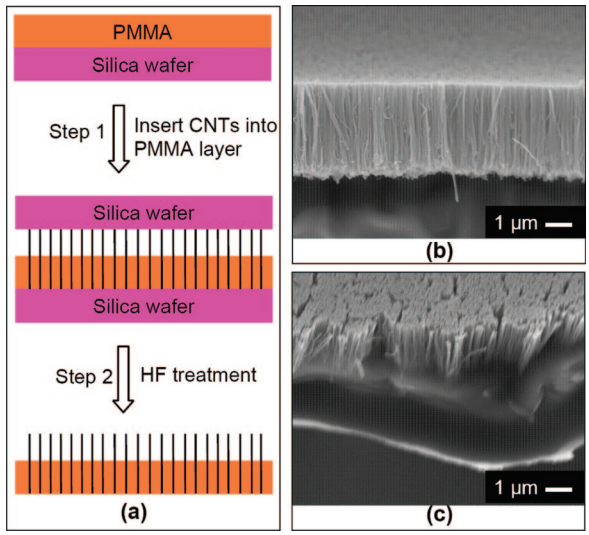

Figure 1. Polymer-embedded VA-CNT array. Schematic illustration of procedures for (a) preparation of the aligned CNTs partially masked by PMMA film and SEM images of (b) the as-synthesized aligned carbon nanotube array and (c) the aligned carbon nanotube array partially embedded into a PMMA film.

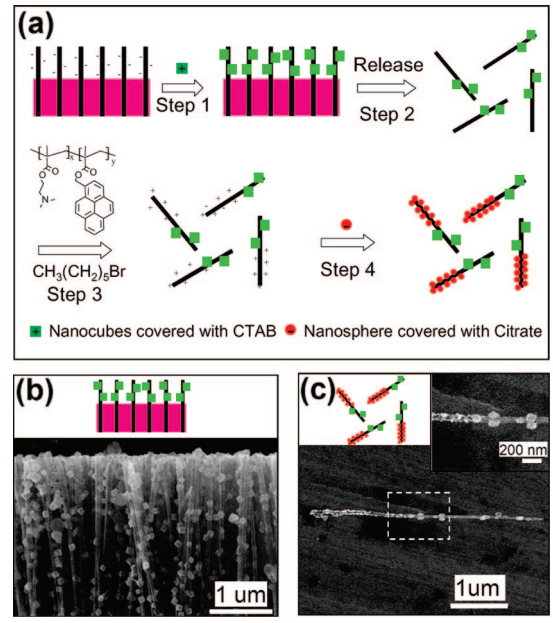

Figure 2. Asymmetric functionalization of CNTs with opposite charges: (a) a schematic representation of procedures for asymmetric functionalization of CNTs with opposite charges, followed by tube-length-specific deposition of gold nanoparticles *via* electrostatic interactions; (b) a schematic representation and SEM image of the CNT array partially functionalized with cubic gold nanoparticles; and (c) a schematic representation and SEM image of the resultant asymmetrically sidewall-functionalized CNTs with half of the nanotube length covered by gold nanocubes and the other half covered by spherical gold nanoparticles through electrostatic assembly. (Inset shows a higher magnification SEM image for the squared area.)

issues on asymmetrical functionalization of CNT tips[34−36] and sidewalls[37] for multifunctional applications.[34−43] In this paper, we report the first approach to *asymmetric* functionalization of individual CNTs with moieties of opposite charges and demonstrate the charge selective adsorption of gold nanoparticles as well as self-assembling of charged carbon nanotubes on electrode surfaces for potential device applications.

RESULTS AND DISCUSSION

We have recently developed a polymer-masking technique for asymmetric functionalization of nanotube sidewalls by sequentially masking vertically aligned carbon nanotubes (VA-CNTs) twice with only half of the nanotube length being modified each time.[37] In that particular case, the controlled polymer-masking with any predetermined embedment length up to the whole nanotube length was achieved by simply heating a polymer thin film on the top of a VA-CNT array for infiltrating the melted polymer chains into the nanotube forest for a certain period of time at an appropriate temperature.[37] Owing to possible thermal fluctuation over the nanotube film, the polymer front may not move downward at a constant speed along all of the constituent aligned CNTs during the infiltration process. In the present study, we developed another polymer-masking technique to allow a more precise control of the embedment length across the whole VA-CNT array by mechanically inserting the VA-CNTs into a spin-cast polymer film with a homogeneous thickness. Figure 1a shows schematically the procedures for preparing a polymer-embeded VA-CNT array through the newly developed polymer-masking method.

In a typical experiment, we first spin-cast a thin layer of poly(methyl methacrylate), PMMA, onto a flat silica wafer from a 40 wt % chloroform solution at a rate of 600 rpm for 2 min (top of Figure 1a). The thickness of the PMMA layer was measured to be ~2.0 μm in this particular case, and it can be regulated by controlling the spin-coating rate and/or polymer concentration. Thereafter, the silica substrate was heated up to a temperature (150 °C) above the glass transition temperature (*ca.* 105 °C) of PMMA, followed by finger pressing an as-grown VA-CNT array into the hot thin polymer film supported by a silica substrate (step 1 of Figure 1a). After having been cooled to room temperature, the silica wafers at both sides were removed in a HF solution (30% w/w) at room temperature.[44] Figure 1b depicts a typical SEM image for the as-synthesized VA-CNT array used in this study. The corresponding SEM image for the polymer-masked VA-CNT array given in Figure 1c clearly shows that the same VA-CNT array has been successfully anchored into the PMMA layer with a homogeneous embedment length of about 1.5 μm.

As schematically shown in Figure 2a, the polymer-free nanotube surface for each of the constituent nanotubes in the PMMA-embedded VA-CNT array was then negatively charged by acetic-acid-plasma polymerization to introduce the carboxylic surface functionalities.[45−47] After the treatment with an aqueous solution of NaOH (0.1 M, Methods) for facilitating the deprotonation of −COOH groups, the plasma treated VA-

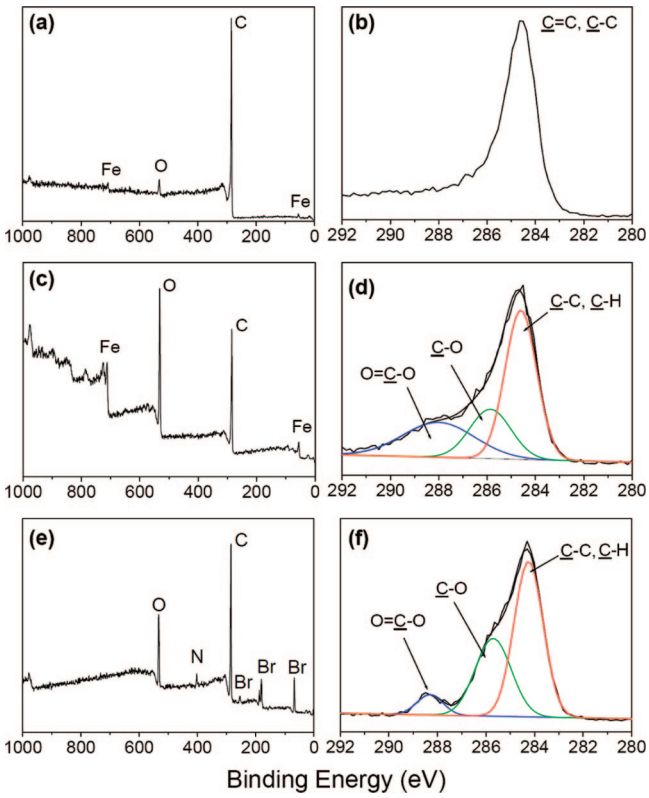

Figure 3. XPS analysis of asymmetric functionalization of CNTs. XPS (a) survey and (b) high-resolution C1s spectrum of the as-grown CNT array, (c) survey, and (d) high-resolution C1s spectrum of the CNT array (half-protected with PMMA polymer) after the acetic-acid-plasma polymerization (see text), (e) survey and (f) high-resolution C1s spectrum of dispersed CNTs with the half-tube-length modified by acetic-acid-plasma polymerization without the NaOH treatment and the other half adsorbed with pyrene-containing copolymer chains after the quaternization treatment with 1-bromohexane (see text).

CNT array was subjected to physical adsorption of positively charged gold nanocubes (Au-NCs) *via* the electrostatic interaction to neutralize the nanotube surface charge (step 1 of Figure 2a). Subsequent removal of the PMMA supporting layer by ultrasonication (VWR model 75D) in chloroform (typically, ~5 min) caused the release of the asymmetrically Au−NC−attached CNTs (step 2 of Figure 2a) for modifying the gold nanoparticle (Au-NP) free surface of the same nanotubes with neutral R_3N-grafted pyrene-DMAEMA (see Scheme 1 and Methods) copolymer chains through the specific pyrene-nanotube interaction (step 3 of Figure 2a). As the areas between the attached Au-NCs along the other half-tube length have been "premasked" by the acetic-acid-plasma polymer coating, its surface interaction with pyrene moieties along the DMAEMA polymer chains is minimal. After quaternization treatment with 1-bromohexane to convert the R_3N groups into positively charged R_4N^+ moieties, negatively charged gold nanospheres (Au-NSs) were finally adsorbed onto the positively charged nanotube surface (step 4 of Figure 2a) *via* the electrostatic interaction. Although the aforementioned asymmetric functionalization principle can be applied to a large variety of charged moieties, the positively charged Au-NCs and negatively charged Au-NSs were used in the present study for easy characterization by SEM visualization.

As expected, the SEM image of the resultant Au−NC-attached CNT array given in Figure 2b clearly shows many gold nanocubes deposited onto the PMMA-free region along the nanotube length while Figure 2c unambiguously reveals the asymmetrically sidewall-modified CNTs with their half-tube-length coated by Au-NCs and the other half-by Au-NSs. The relatively low number of Au-NCs along individual CNTs seen in Figure 2c with respect to Figure 2b indicates, most probably, that some of the adsorbed Au-NCs have been removed from the nanotube surface during the process to dissolve the PMMA protective layer and the subsequent solution steps shown in Figure 2a.

To confirm the effectiveness of the nanotube modification steps, Figure 3 summarizes the XPS survey and high-resolution C1s spectra. As expected for the as-grown CNT array (Figure 3a,b), the XPS survey spectrum shows a C 1s peak around 285 eV and O 1s peak at 531 eV, presumably arising from physically adsorbed oxygen-containing species.[46] The Fe signals at about 55 and 707 eV were attributable to the residual catalyst in the FePc-generated VA-CNTs.[46,48] The corresponding XPS survey spectrum for the PMMA-supported and acetic-acid-plasma-treated VA-CNT array (Figure 3c) shows similar peaks as Figure 3a, but

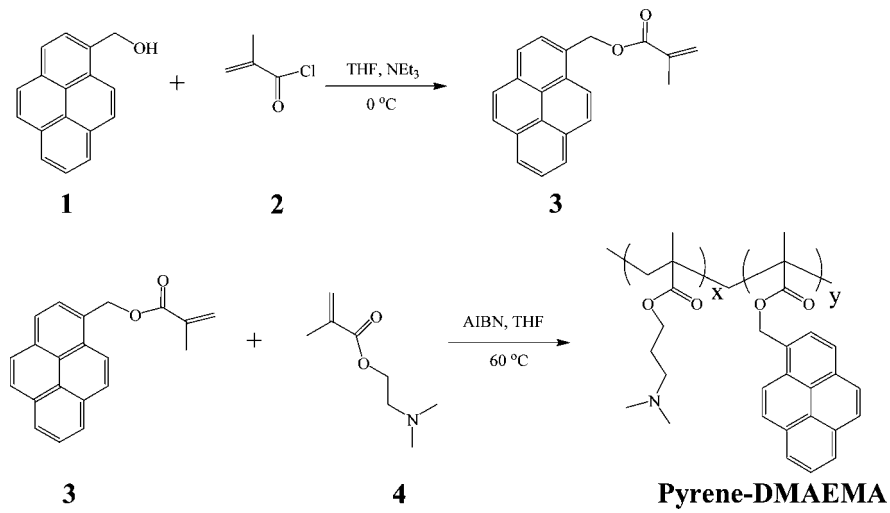

Scheme 1

with a significantly increased O/C atomic ratio. These features are consistent with the treatments shown in Figure 2a. As plasma polymerization is always accompanied by certain degree of plasma etching,[49,50] the increase in Fe signal shown in Figure 3c with respect to Figure 3a is presumably due to the preferential removal of carbon structure at the nanotube tips to expose residual Fe catalyst nanoparticles at the top of the aligned CNT array.[48,51,52] The high-resolution C1s spectrum of the as-grown VA-CNT array (Figure 3b) shows a relatively narrow graphitic C at about 285 eV,[46] whereas the corresponding high-resolution C1s spectrum for the PMMA-supported and acetic-acid-plasma-treated VA-CNT array given in Figure 3d shows three peak components at 284.6, 286.2, and 288.5 eV, which are assigned to the C−C or C−H, C−O and O═C−O components, respectively, in the acetic-acid-plasma polymer. Thus, the XPS spectra shown in Figure 3c,d clearly indicated that the PMMA-free surface of the VA-CNTs had been modified with the COOH groups.

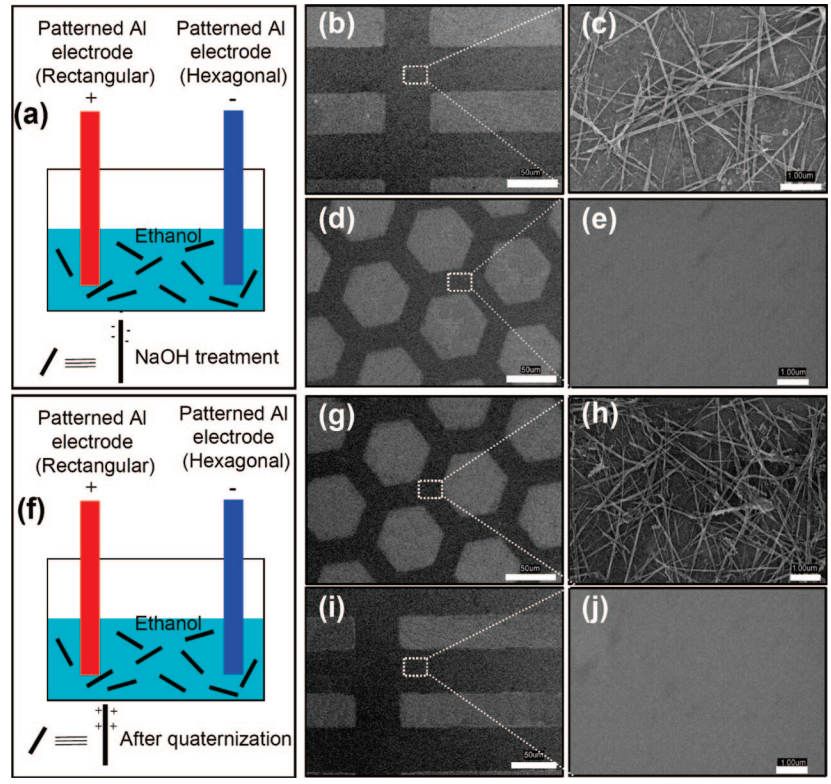

Figure 4. Selective deposition of asymmetric functionalization of CNTs. (a) A schematic illustration of the experimental setup for selective deposition of CNTs, with their half-tube-length negatively charged by acetic-acid-plasma polymer after NaOH treatment (see text), onto a rectangularly patterned positive Al electrode; (b) an SEM image of the rectangularly patterned positive Al electrode after having been immersed into the CNT solution shown in panel a for 5 min under 10 V; (c) an enlarged view of an area on the Al rectangular network in panel b; (d) an SEM image of the hexagonally patterned negative Al electrode after having been immersed into the CNT solution shown in panel a for 5 min under 10 V; (e) an enlarged view of the square area on the Al hexagonal network in panel d; (f) a schematic illustration of the experimental setup for selective deposition of CNTs, with their half-tube-length positively charged by pyrene-DMAEMA after quaternization (see text), onto a hexagonally patterned negative Al electrode; (g) an SEM image of hexagonally patterned negative Al electrode after having been immersed into the CNT solution shown in panel f for 5 min under 10 V; (h) an enlarged view of an area on the Al hexagonal network in panel g; (i) an SEM image of the rectangular-patterned positive Al electrode after having been immersed into the CNT solution shown in panel f for 5 min under 10 V; (j) an enlarged view of the square area on the Al rectangular network in panel i. Scale bars: (b, d, g, i), 50 μm; (c, e, h, j), 1 μm.

For the preparation of a half-positively charged nanotube, the acetic-acid-plasma polymerized CNTs were freed from the PMMA protection by washing thoroughly with acetone and redispersing in an aqueous solution of R_3N-grafted pyrene-DMAEMA copolymer (Scheme 1, 20 mg/100 mL) for physical adsorption of the polymer chains *via* the π−π stacking interaction between pyrene moieties and the free nanotube surface, followed by quaternization treatment with 1-bromohexane (*vide supra*). Figure 3 panels e and f show the XPS survey and C1s spectra for the resulting half-positively charged and half-plasma-treated nanotubes. As seen in Figure 3e, the XPS survey spectrum shows a C 1s peak at 285, O 1s peak at 531, and N 1s peak at 402 eV. The enhanced C/O atomic ratio seen in Figure 3e with respect to that of Figure 3c reflects the high atomic ratio of C/O for the newly adsorbed pyrene-DMAEMA chains. In addition, three new peaks appeared at about 68, 181, and 255 eV, respectively, arising from the Br counterions after the quaternization treatment with 1-bromohexane (step 3 of Figure 2a and Methods).

Comparing with Figure 3a,c, the absence of Fe peaks in Figure 3e indicates, most probably, that the exposed residue Fe catalyst particles at the nanotube tips have been physically removed during the solution process to free the CNTs from PMMA protection and subsequent solution process. The corresponding XPS C1s spectrum of the asymmetrically functionalized CNTs with the acetic-acid-plasma polymer and quaternized pyrene-DMAEMA chains is given in Figure 3f, which shows three peak components at about 284.6, 286.2, and 288.5 eV attributable to the C−C or C−H, C−O and O═C−O species, respectively. Therefore, the above XPS results suggested, once again, the asymmetric functionaliza-

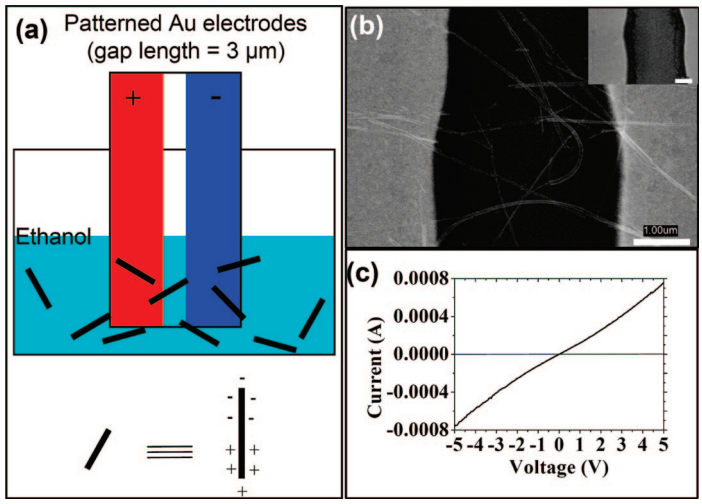

Figure 5. Self-assembly of asymmetric functionalization of CNTs. (a) A schematic illustration of the experimental setup for self-assembling CNTs, with their half-tube-length functionalized by pyrene-DMAEMA copolymer chains containing R_3HN^+ moieties and the other half-tube-length by the plasma polymer containing COO^- moieties (see text), onto two parallel electrodes less than 3-μm apart under a DC voltage; (b) An SEM image of the patterned Au electrodes after having been immersed into the CNT solution shown in panel a for 10 min under 10 V. Insert at the top-right corner shows the corresponding SEM image obtained from a control experiment with noncharged CNTs; (c) A typical current−voltage curve for the CNTs self-assembled between the two Au electrodes shown in panel b. Scale bar (b): 1 μm.

tion of the CNTs with the quaternized pyrene-DMAEMA chains of positively charged R_4N^+ groups associated with Br^- counterions along a half-length of the nanotube sidewall and negatively chargeable acetic-acid-plasma-polymer coating on the other half-sidewall for each of the individual CNTs (*vide infra*).

The resultant asymmetrically sidewall-functionalized CNTs can then be used for region-specific adsorption of Au−NSs and Au−NCs, as described above. In addition to providing a platform for site-specific assembly on the CNT surface, the asymmetric sidewall-functionalization facilitates incorporation of the CNT into device architectures. Figure 4 summarizes results of charge-specific adsorption of these CNTs onto micropatterned aluminum (Al) electrodes on silica wafers (see, Methods). Here, the asymmetrically acetic-acid-plasma-treated CNTs released from the PMMA mask with half-tube length negatively charged and half-neutral were used. The half-tube-length negatively charged CNTs were dispersed in ethanol within an electrochemical cell containing two well-separated Al micropatterned electrodes (Figure 4a). Upon applying a DC voltage of 10 V on the two micropatterned Al electrodes for 5 min, we found that the negatively charged CNTs selectively adsorbed onto the rectangularly micropatterned Al positive electrode (Figure 4b,c), but not on the hexagonally micropatterned Al negative electrode (Figure 4d,e).

We further tested the charge-selective adsorption for CNTs with their half-tube-length asymmetrically sidewall-functionalized by R_3N-grafted pyrene-DMAEMA copolymer chains after quaternization treatment with 1-bromohexane to convert the R_3N groups into positively charged R_4N^+ moieties with the other half of the VA-CNT array having been protected by the PMMA coating. The resultant half-tube-length positively charged CNTs were released from the PMMA mask and dispersed in ethanol within an electrochemical cell containing two well-separated Al micropatterned electrodes (Figure 4f). By applying the same DC voltage (10 V) as used in Figure 4a onto the two micropatterned Al electrodes shown in Figure 4f for 5 min, we found in this particular case that the positively charged CNTs selectively adsorbed onto the hexagonally micropatterned Al negative electrode (Figures 4g, h), but not on the rectangularly micropatterned Al positive electrode (Figures 4i, j). In both cases, no carbon nanotube adsorption on either of the two electrodes was observed in control experiments when no external voltage was applied.

The above observations prompted us to use the charge-selective adsorption for self-assembling the asymmetrically sidewall-charged CNTs across two photolithographically patterned parallel electrodes (e.g., Au) of a narrow gap less than 3-μm wide by applying a DC voltage with opposite biases for the Au electrodes. As shown in Figure 5a, the asymmetrically sidewall-charged CNTs, with their half-tube-length functionalized by pyrene-DMAEMA copolymer chains containing R_3HN^+ moieties and the other half-tube-length by the plasma polymer containing COO moieties, were dispersed in ethanol within an electrochemical cell containing a silica wafer photolithographically patterned with two parallel electrodes less than 3-μm apart (Figure 5a). After the application of a DC voltage (10 V) between the two electrodes for 10 min, we took the silica wafer out of the electrochemical cell and thoroughly washed it with pure ethanol, followed by air drying at room temperature. SEM examination of the resultant electrodes revealed that some of the asymmetrically sidewall-charged CNTs have been well registered between the two electrodes (Figure 5b), presumably by simultaneously adsorbing their positively charged side onto the negative electrode and negatively charged side onto the positive electrode. This is, at least partially, confirmed by the absence of CNT adsorption in control experiments, in which either noncharged CNTs were used or no external voltage was applied onto the two electrodes immersed in the asymmetrically charged CNT solution (cf. insert of Figure 5b) under the same conditions, though prolonged adsorption under an applied voltage could lead to assem-

bly of some unfunctionalized CNTs between the two electrodes.

It is important to point out here that the number of the asymmetrically charged CNTs and their alignment for CNTs to be adsorbed across the two electrodes can be regulated by adjusting the deposition conditions, such as nanotube concentration, deposition time, intensity of the applied voltage, and with or without shear. Also, the pristine nanotube surface structure could be restored by thermal decomposition of the grafted moieties under vacuum.[2] Although the unoptimized CNT electric circuit shown in Figure 5b is not ideal for practical applications, its current (I)−voltage (V) characteristics (Figure 5c) show a pseudolinear $I-V$ curve consistent with a non-ohmic contact between the CNT and electrode arising from the dielectric polymeric layer on the CNT surface.[2] It is worth pointing out here that the methodology developed in this study can be used to asymmetrically functionalize both multiwalled and single-walled carbon nanotubes with moieties of opposite charges. With various techniques already reported, and more to be developed, for preferential syntheses and purification of semiconducting single-walled carbon nanotubes,[2,53] there will be vast opportunities for the asymmetrically charged semiconducting single-walled carbon nanotubes to be used as building blocks in various nanotube devices.

In summary, we have demonstrated a simple, but effective, asymmetric modification of the sidewall of CNTs with oppositely charged moieties by plasma treatment and $\pi-\pi$ stacking interaction. The *as-prepared* asymmetrically sidewall-functionalized CNTs can be used as a platform for bottom-up self-assembly of complex structures or can be charge-selectively self-assembled onto and/or between electrodes with specific biases under an appropriate applied voltage for device applications. Owing to the highly generic nature characteristic of the plasma technique, together with the versatile $\pi-\pi$ stacking interaction between the pyrene-grafted molecules and CNT surface, the methodology developed in this study could be regarded as a general approach toward fabricating asymmetrically charged carbon nanotubes for many potential applications, ranging from nanotube electronic devices to biomedical systems.

METHODS

Syntheses of Aligned Carbon Nanotubes. The VA-CNTs were prepared by pyrolysis of iron(II) phthalocyanine (FePc) under a Ar/H_2 flow at 800−1100 °C, according to our reported procedures.[44] The FePc-generated VA-CNTs are multiwalled nanotubes, typically having a well-graphitized structure with *ca.* 50 concentric carbon shells and an outer diameter of *ca.* 40 nm.[44,48]

Acetic Acid Plasma Polymerization. The acetic-acid-plasma polymerization onto PMMA embedded VA-CNT arrays was performed on a custom-built plasma apparatus powered at 250 kHz, 30 W, and a monomer pressure of 0.1 Torr for 1 min.[45,46] The resulting plasma-treated VA-CNT array was then immersed into an aqueous solution of NaOH (0.1 M) for 30 min to convert the plasma-induced COOH groups into COO^- moieties to charge the CNT surface negatively.

Synthesis of (1-Pyrene) Methyl-2-methyl-2-propenoate (3). Scheme 1 shows the reaction route used for the preparation of pyrene-functionalized poly(dimethylaminoethyl methacrylate), pyrene-DMAEMA. To start with, methacryloyl chloride (**2**) (3.15 mL; 0.032 mol) was added dropwise into a mixture of 1-pyrenemethanol (**1**) (2.50 g; 0.011 mol) and triethylamine (4.50 mL; 0.032 mol) in 100 mL of dry THF under stirring at 0 °C. The reaction was carried out at room temperature for 24 h, and the resulting mixture was filtered. The solid residue obtained after evaporation of THF was dissolved in 200 mL of methylene chloride, followed by sequential washing with 0.5 M HCl solution, 0.2 M $NaHCO_3$ solution, and pure water. After drying with $MgSO_4$ and evaporation of the solvent under reduced pressure, the crude yellow product was purified by column chromatography over silica gel, eluting with methylene chloride to afford compound **3** with a yield of 80%. ^{1}H NMR(300 MHz, $CDCl_3$, δ): 8.03−8.33 (m, 9H, aromatic H), 6.15 (s, 1H, CH_2═C), 5.90 (s, 2H, CH_2O), 5.56 (s, 1H, CH_2═C), 1.97 (s, 3H, CH_3). Anal. Calcd for $C_{21}H_{16}O_2$: C, 84.00; H, 5.33; O, 10.67. Found: C, 82.98; H, 5.33; O, 10.79.

Synthesis of Pyrene-Based Copolymer (Pyrene-DMAEMA). A mixture of compound **3** (0.50 g, 1.70 mmol), dimethylaminoethyl methacrylate (**4**) (5.81 g, 37 mmol) and AIBN initiator (0.04 g, 0.24 mmol) was dissolved into 5 mL of dry THF in a glass polymerization tube (Scheme 1). The homogeneous solution was purged with argon for 10 min and sealed under a reduced argon atmosphere. The copolymerization was carried out with continuous stirring at 60 °C for 48 h. The viscous solution was then diluted with 5 mL of THF and precipitated into 100 mL of hexane under vigorous stirring. The resulting solid material was collected by filtration and dried under reduced pressure. The copolymer product was further purified by Soxhlet extraction with boiling hexane for 24 h and finally dried in a vacuum oven at 50 °C for 24 h, leading to the production of R_3N-grafted pyrene-DMAEMA with a yield of 62%. After the GPC and NMR characterization (see below), the resultant copolymer was subjected to the quaternization treatment with 1-bromohexane, according to a published procedure,[54] to convert the R_3N groups into positively charged R_4N^+ moieties. M_n = 11600 g/mol; M_w/M_n = 2.03. ^{1}H NMR($CDCl_3$, δ): 8.0−8.2 (broad, m, weak), 5.80 (broad, s, weak), 4.08 (broad, s, medium), 2.56 (broad, s, medium), 2.15−2.27 (broad, m, strong), 1.83−1.91 (broad, m, medium), 0.89−1.37 (broad, m, medium).

Synthesis of Positively Charged Gold Nanoparticles. The cubic gold nanoparticles (90 nm; designated as Au-NCs) with positively charged surface (covered with a layer of cetyltrimethylammonium bromide, CTBA) were prepared according to the previously reported procedures.[55] In particular, cubic gold sols were synthesized *via* a gold seed growth reaction. For the gold seed preparation, $HAuCl_4 \cdot 3H_2O$ (2.5×10^{-4} M) was reduced with ice-cold $NaBH_4$ (6.0×10^{-4} M) in the presence of cetyltrimethylammonium bromide (CTAB, 7.5×10^{-2} M). After the addition of $NaBH_4$ to the aqueous solution (10 mL) containing CTAB and $HAuCl_4$, the reaction mixture was stirred for 2 min. These seeds are less than 2 nm in diameter. In a typical cubic Au nanoparticle growth reaction, 0.40 mL of $HAuCl_4$ solution (0.005 M) was added to 4.75 mL of CTAB solution (0.10 M) followed by the addition of 0.03 mL of $AgNO_3$ (0.01 M), 0.034 mL of Lascorbic acid (0.10 M), and 0.01 mL of Au seed solutions. The solution was gently mixed by inversion of the test tube immediately after the addition of every component each time. The edge length of the cubic gold nanoparticles thus prepared is about 90 nm. These positive Au-NCs were used for charge-selective adsorption onto negatively charged VA-CNTs through the highly specific electrostatic interaction (*vide supra*).

Synthesis of Negatively-Charged Gold Nanoparticles. An aqueous solution of $HAuCl_4$ (10 mL; 2×10^{-3} M) was refluxed under stirring. To the boiling $HAuCl_4$ solution was added an aqueous solution of trisodium citrate (10 mL; 8×10^{-3} M). The mixture solution of $HAuCl_4$ and trisodium citrate was then refluxed for 15 min to cause a slow color change from gray to pale red. Af-

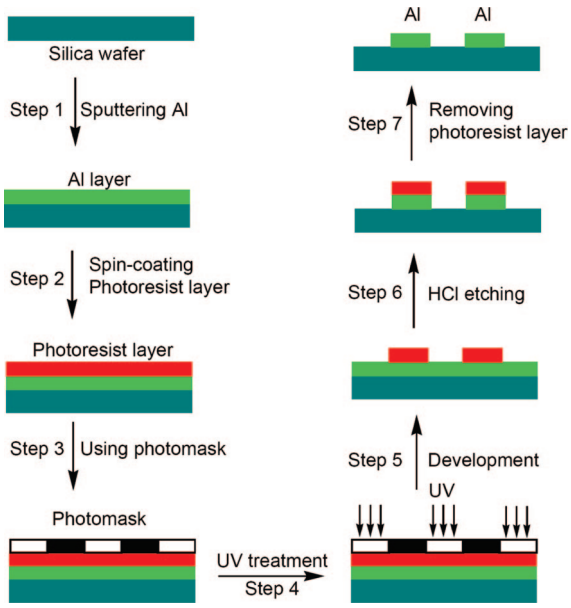

Figure 6. Preparation of Al microelectrodes. A schematic representation of procedures for the micropattern formation of aluminum (Al) electrodes by photolithographic patterning.

ter further boiling for 15 min, the reaction solution was cooled down to room temperature to produce a wine-red solution of spherical gold nanoparticles (Au-NSs). The *as-prepared* gold nanospheres have a diameter of ~10 nm.

Preparation of Patterned Electrodes. The photolithographic procedure shown in Figure 6 is self-explanatory and allows the formation of both rectangularly shaped and hexagonally shaped aluminum (Al) micropatterns on silica wafers by using TEM grid masks with rectangular and hexagonal windows, respectively. Specifically, a thin (1.1 μm) layer of AZ3312 photoresist (AZ Electronic Materials USA Corp.) was spin-deposited (400 rpm, step 2 of Figure 6) onto the sputter-coated Al film (step 1 of Figure 6), followed by UV light exposure through a TEM grid (steps 3 and 4 of Figure 6) and washing with the developer (AZ300 MIF, AZ Electronic Materials USA Corp., step 5 of Figure 6) and an aqueous HCl solution (0.1 M, step 6 of Figure 6) to sequentially remove the photoresist and Al within the exposed areas. Finally, the photoresist layer in the unexposed regions was removed by acetone washing to produce Al micropattern on the silica wafer (step 7 of Figure 6).

Characterization. Scanning electron microscope (SEM) imaging was performed on a Hitachi S-4800 high-resolution SEM unit. X-ray photoelectron spectroscopic (XPS) measurements were made on a VG Microtech ESCA 2000 using monochromatic Mg Kα radiation at a power of 300 W. ^{1}H NMR spectra were recorded on a Bruker Avance 3000 spectrometer with *d*-chloroform as the solvent and tetramethylsilane as the internal standard. Number-average (M_n) molecular weights were determined on a Viscotek GPC system (a model 250 RI/viscosity detector). *I*−*V* measurements were performed on an Agilent 4156C semiconductor analyzer.

Acknowledgment. We are grateful for partial support from AFRL/RX (LDF), AFOSR (FA9550-06-1-0384), NSF (NIRT 0609077; CMS-078055), and WBI (PIA FA8652-03-3-0005). We acknowledge the NEST Laboratory at UD for access to the SEM and TEM facilities.

REFERENCES AND NOTES

1. Iijima, S. Helical Microtubules of Graphitic Carbon. *Nature* **1991**, *354*, 56–58.
2. *Carbon Nanotechnology: Recent Developments in Chemistry, Physics, Materials Science and Device Applications*; Dai, L. Ed.; Elsevier: Amsterdam, 2006.
3. Collins, P. G.; Zettl, A.; Bando, H.; Thess, A.; Smalley, R. E. Nanotube Nanodevice. *Science* **1997**, *278*, 100–102.
4. Tans, S. J.; Devoret, M. H.; Dai, H. J.; Thess, A.; Smalley, R. E.; Geerligs, L. J.; Dekker, C. Individual Single-wall Carbon Nanotubes as Quantum Wires. *Nature* **1997**, *386*, 474–477.
5. Treacy, M. M. J.; Ebbesen, T. W.; Gibson, J. M. Exceptionally High Young's Modulus Observed for Individual Carbon Nanotubes. *Nature* **1996**, *381*, 678–680.
6. Kong, J.; Franklin, N. R.; Zhou, C. W.; Chapline, M. G.; Peng, S.; Cho, K. J.; Dai, H. J. Nanotube Molecular Wires as Chemical Sensors. *Science* **2000**, *287*, 622–625.
7. Planeix, J. M.; Coustel, N.; Coq, B.; Brotons, V.; Kumbhar, P. S.; Dutartre, R.; Geneste, P.; Bernier, P.; Ajayan, P. M. Application of Carbon Nanotubes as Supports in Heterogeneous Catalysis. *J. Am. Chem. Soc.* **1994**, *116*, 7935–7936.
8. Baughman, R. H.; Zakhidov, A. A.; de Heer, W. A. Carbon Nanotubes - The Route Toward Applications. *Science* **2002**, *297*, 787–792.
9. Ajayan, P. M.; Tour, J. M. Materials Science: Nanotube Composites. *Nature* **2007**, *447*, 1066–1068.
10. Qu, L.; Peng, Q.; Dai, L.; Spinks, G. M.; Wallace, G. G.; Baughman, R. H. Carbon Nanotube Electroactive Polymer Materials: Opportunities and Challenges. *MRS Bull.* **2008**, *33*, 215–224.
11. Sun, Y. P.; Huang, W.; Lin, Y.; Fu, K.; Kitaygorodskiy, A.; Riddle, L. A.; Yu, Y. J.; Carroll, D. L. Soluble Dendron-Functionalized Carbon Nanotubes: Preparation, Characterization, and Properties. *Chem. Mater.* **2001**, *13*, 2864–2869.
12. Huang, W.; Lin, Y.; Tayler, S.; Gaillard, J.; Rao, A. M.; Sun, Y. P. Sonication-Assisted Functionalization and Solubilization of Carbon Nanotubes. *Nano. Lett.* **2002**, *2*, 231–234.
13. Shim, M.; Kam, W. S. K.; Chen, R. J.; Li, Y.; Dai, H. J. Functionalization of Carbon Nanotubes for Biocompatibility and Biomolecular Recognition. *Nano. Lett.* **2002**, *2*, 285–288.
14. Zheng, M.; Jagota, A.; Semke, E. D.; Diner, B. A.; Mclean, R. S.; Lustig, S. R.; Richardson, R. E.; Tassi, N. G. DNA-Assisted Dispersion and Separation of Carbon Nanotubes. *Nat. Mater.* **2003**, *2*, 338–342.
15. Lin, T.; Ji, T.; Bajpai, V.; Dai, L. Chemistry of Carbon Nanotubes. *J. Aust. Chem.* **2003**, *56*, 635–651.
16. Tasis, D.; Tagmatarchis, N.; Bianco, A.; Prato, M. Chemistry of Carbon Nanotubes. *Chem. Rev.* **2006**, *106*, 1105–1136.
17. Zhao, W.; Song, C.; Pehrsson, P. E. Water-Soluble and Optically pH-Sensitive Single-Walled Carbon Nanotubes from Surface Modification. *J. Am. Chem. Soc.* **2002**, *124*, 12418–12419.
18. Paloniemi, H.; Aaritalo, T.; Laiho, T.; Liuke, H.; Kocharova, N.; Haapakka, K.; Terzi, F.; Seeber, R.; Lukkari, J. Water-Soluble Full-Length Single-Wall Carbon Nanotube Polyelectrolytes: Preparation and Characterization. *J. Phys. Chem. B* **2005**, *109*, 8634–8642.
19. Chen, R. J.; Zhang, Y.; Wang, D.; Dai, H. J. Noncovalent Sidewall Functionalization of Single-Walled Carbon Nanotubes for Protein Immobilization. *J. Am. Chem. Soc.* **2001**, *123*, 3838–3839.
20. Guldi, D. M.; Rahman, G. M. A.; Jux, N.; Tagmatarchis, N.; Prato, M. Integrating Single-Wall Carbon Nanotubes into Donor−Acceptor Nanohybrids. *Angew. Chem., Int. Ed.* **2004**, *43*, 5526–5530.
21. Zhang, J.; Lee, J. K.; Wu, Y.; Murray, R. W. Photoluminescence and Electronic Interaction of Anthracene Derivatives Adsorbed on Sidewalls of Single-Walled Carbon Nanotubes. *Nano Lett.* **2003**, *3*, 403–407.
22. Curran, S. A.; Ajayan, P. M.; Blau, W. J.; Carroll, D. L.; Coleman, J. N.; Dalton, A. B.; Davey, A. P.; Drury, A.; McCathy, B.; Maier, S.; *et al.* A Composite from Poly(*m*-phenylenevinylene-*co*-2,5-dioctoxy-*p*-phenylenevinylene) and Carbon Nanotubes: A Novel Material for Molecular Optoelectronics. *Adv. Mater.* **1998**, *10*, 1091–1093.

23. Tang, B. Z.; Xu, H. Y. Preparation, Alignment, and Optical Properties of Soluble Poly(phenylacetylene)-Wrapped Carbon Nanotubes. *Macromolecules* **1999**, *32*, 2569–2576.
24. Li, C. Y.; Li, L.; Cai, W.; Kodjie, S. L.; Tenneti, K. K. Nanohybrid Shish-Kebabs: Periodically Functionalized Carbon Nanotubes. *Adv. Mater.* **2005**, *17*, 1198–1202.
25. Li, J.; Ng, H. T.; Cassell, A.; Fan, W.; Chen, H.; Ye, Q.; Koehne, J.; Han, J.; Meyyappan, M. Carbon Nanotube Nanoelectrode Array for Ultrasensitive DNA Detection. *Nano. Lett.* **2003**, *3*, 597–602.
26. Chen, W.; Dai, L.; Roy, A.; Tolle, T. B. Multifunctional Chemical Vapor Sensors of Aligned Carbon Nanotube and Polymer Composites. *J. Am. Chem. Soc.* **2006**, *128*, 1412–1413.
27. Dai, J.; Jensen, A. W.; Mohanty, D. K.; Erndt, J.; Bruening, M. L. Controlling the Permeability of Multilayered Polyelectrolyte Films through Derivatization, Cross-Linking, and Hydrolysis. *Langmuir* **2001**, *17*, 931–937.
28. Farhet, T. R.; Schlenoff, J. B. Ion Transport and Equilibria in Polyelectrolyte Multilayers. *Langmuir* **2001**, *17*, 1184–1192.
29. Eckle, M.; Decher, G. Tuning the Performance of Layer-by-Layer Assembled Organic Light Emitting Diodes by Controlling the Position of Isolating Clay Barrier Sheets. *Nano Lett.* **2001**, *1*, 45–49.
30. Jung, Y. J.; Kar, S.; Talapatra, S.; Soldano, C.; Viswanathan, G.; Li, X. S.; Yao, Z. L.; Ou, F. S.; Avadhanula, A.; Vajtai, R.; *et al.* Aligned Carbon Nanotube-Polymer Hybrid Architectures for Diverse Flexible Electronic Applications. *Nano. Lett.* **2006**, *6*, 413–418.
31. Choi, H. C.; Shim, M.; Bangsaruntip, S.; Dai, H. J. Spontaneous Reduction of Metal Ions on the Sidewalls of Carbon Nanotubes. *J. Am. Chem. Soc.* **2002**, *124*, 9058–9059.
32. Jiang, K. Y.; Eitan, A.; Schadler, L. S.; Ajayan, P. M.; Siegel, R. W. Selective Attachment of Gold Nanoparticles to Nitrogen-Doped Carbon Nanotubes. *Nano. Lett.* **2003**, *3*, 275–277.
33. Carrillo, A.; Swartz, J. A.; Gamba, J. M.; Kane, R. S.; Chakrapani, N. M.; Wei, B. Q.; Ajayan, P. M. Noncovalent Functionalization of Graphite and Carbon Nanotubes with Polymer Multilayers and Gold Nanoparticles. *Nano Lett.* **2003**, *3*, 1437–1440.
34. Majumder, M.; Chopra, N.; Hinds, B. J. Effect of Tip Functionalization on Transport through Vertically Oriented Carbon Nanotube Membranes. *J. Am. Chem. Soc.* **2005**, *127*, 9062–9070.
35. Lee, K. M.; Li, L. C.; Dai, L. Asymmetric End-Functionalization of Multi-Walled Carbon Nanotubes. *J. Am. Chem. Soc.* **2005**, *127*, 4122–4123.
36. Chopra, N.; Majumder, M.; Hinds, B. J. Bifunctional Carbon Nanotubes by Sidewall Protection. *Adv. Funct. Mater.* **2005**, *15*, 858–864.
37. Qu, L.; Dai, L. Polymer-Masking for Controlled Functionalization of Carbon Nanotubes. *Chem. Commun.* **2007**, 3859–3861.
38. Burghard, M. Asymmetric End-Functionalization of Carbon Nanotubes. *Small* **2005**, *1*, 1148–1150.
39. Banerjee, S.; Wong, S. S. Synthesis and Characterization of Carbon Nanotube-Nanocrystal Heterostructures. *Nano. Lett.* **2002**, *2*, 195–200.
40. Sun, J.; Iwasa, M.; Gao, L.; Zhang, Q. Single-Walled Carbon Nanotubes Coated with Titania Nanoparticles. *Carbon* **2004**, *42*, 895–899.
41. Chiu, P. W.; Duesberg, G. S.; Weglikowska, U. D.; Roth, S. Interconnection of Carbon Nanotubes by Chemical Functionalization. *Appl. Phys. Lett.* **2002**, *80*, 3811–3813.
42. Katz, E.; Willner, I. Biomolecule-Functionalized Carbon Nanotubes: Applications in Nanobioelectronics. *Chemphyschem* **2004**, *5*, 1084–1104.
43. Imahori, H.; Mori, Y.; Matano, Y. Nanostructured Artificial Photosynthesis. *J. Photochem. Photobiol. C* **2003**, *4*, 51–83.
44. Huang, S.; Dai, L.; Mau, A. W. H. Patterned Growth and Contact Transfer of Well-Aligned Carbon Nanotube Films. *J. Phys. Chem.* **1999**, *103*, 4223–4227.
45. Chen, Q.; Dai, L. Plasma Patterning of Carbon Nanotubes. *Appl. Phys. Lett.* **2000**, *76*, 2719–2721.
46. Chen, Q.; Dai, L.; Gao, M.; Huang, S.; Mau, A. Plasma Activation of Carbon Nanotubes for Chemical Modification. J. Phys. Chem. B **2001**, *105*, 618−622, and references cited therein.
47. He, P.; Dai, L. Aligned Carbon Nanotube−DNA Electrochemical Sensors. *Chem. Commun.* **2004**, 348–349.
48. Li, D. C.; Dai, L.; Huang, S.; Mau, A. W. H.; Wang, Z. L. Structure and Growth of Aligned Carbon Nanotube Films by Pyrolysis. *Chem. Phys. Lett.* **2000**, *316*, 349–355.
49. Yasuda, H. *Plasma Polymerization*; Academic Press: New York, 1985.
50. *Plasma Deposition, Treatment, and Etching of Polymers*; d'Agostino, R., Ed.; Academic Press: New York, 1990.
51. Huang, S.; Dai, L. Plasma Etching for Purification and Controlled Opening of Aligned Carbon Nanotubes. *J. Phys. Chem. B* **2002**, *106*, 3543–3545.
52. *Methods of Surface Analysis: Techniques and Applications*; Walls, J. M., Ed.; Cambridge University Press: Cambridge, U.K., 1990.
53. Qu, L.; Du, F.; Dai, L. Preferential Syntheses of Semiconducting Vertically-Aligned Single-Walled Carbon Nanotubes for Direct Use in FETs. Nano Lett. Published online July 30, 2008, http://dx.doi.org/10.1021/nl800967n (and references cited therein).
54. Cheng, Z. P.; Zhu, X. L.; Shi, Z. L.; Neoh, K. G.; Kang, E. T. Polymer Microspheres with Permanent Antibacterial Surface from Surface-Initiated Atom Transfer Radical Polymerization. *Ind. Eng. Chem. Res.* **2005**, *44*, 7098–7104.
55. Sau, T. K.; Catherine, J.; Murphy, C. J. Room Temperature, High-Yield Synthesis of Multiple Shapes of Gold Nanoparticles in Aqueous Solution. *J. Am. Chem. Soc.* **2004**, *126*, 8648–8649.